PCCP

ROYAL SOCIETY OF CHEMISTRY

ARTICLE TYPE

Cite this: DOI: 10.1039/xxxxxxxxxx

Coordination of the Biliverdin D-ring in Bacteriophytochromes

Nils Lenngren,[a‡] Petra Edlund,[b‡] Heikki Takala,[a,c‡] Brigitte Stucki-Buchli,[a] Jessica Rumfeldt,[a] Ivan Peshev,[a] Heikki Häkkänen,[a] Sebastian Westenhoff,*[b] and Janne A. Ihalainen*[a]

Received Date
Accepted Date

DOI: 10.1039/xxxxxxxxxx

www.rsc.org/journalname

Phytochrome proteins translate light into biochemical signals in plants, fungi and microorganisms. Light cues are absorbed by a bilin chromophore, leading to an isomerization and a rotation of the D-ring. This relays the signal to the protein matrix. A set of amino acids, which is conserved across the phytochrome superfamily, holds the chromophore in the binding pocket. However, the functional role of many of these amino acids is not yet understood. Here, we investigate the hydrogen bonding network which surrounds the D-ring of the chromophore in the resting (Pr) state. We use UV/Vis spectroscopy, infrared absorption spectroscopy and X-ray crystallography to compare the photosensory domains from *Deinococcus radiodurans*, the phytochrome 1 from *Stigmatella aurantiaca*, and a *D. radiodurans* H290T mutant. In the latter two, an otherwise conserved histidine next to the D-ring is replaced by a threonine. Our infrared absorption data indicate that the carbonyl of the D-ring is more strongly coordinated by hydrogen bonds when the histidine is missing. This is in apparent contrast with the crystal structure of the PAS-GAF domain of phytochrome 1 from *S. aurantiaca* (pdb code 4RPW), which did not resolve any obvious binding partners for the D-ring carbonyl. We present a new crystal structure of the H290T mutant of the PAS-GAF from *D. radiodurans* phytochrome. The 1.4- Å-resolution structure reveals additional water molecules, which fill the void created by the mutation. Two of the waters are significantly disordered, suggesting that flexibility might be important for the photoconversion. Finally, we report a spectral analysis which quantitatively explains why the histidine-less phytochromes do not reach equal Pfr -type absorption in the photoequilibrium compared to the *Deinococcus radiodurans* wild-type protein. The study highlights the importance of water molecules and the hydrogen bonding network around the chromophore for controlling the isomerization reaction and spectral properties of phytochromes.

1 Introduction

Phytochromes are photosensor proteins in plants,[1] bacteria,[2–6] and fungi.[7] The proteins sense ambient light levels and control the developmental processes in the organisms.[8–10] Most phytochromes detect red and far-red light, but variants in photosynthetic bacteria are tuned to sense other colors of the visible spectral region.[11] Upon light absorption, a bilin chromophore isomerizes around the bond connecting the C- and D-rings.[12,13] This triggers a series of photochemical and structural changes,[14] which finally results in modification of the biochemical activity of the protein.

In canonical phytochromes, the resting state is called Pr, after its red-light absorption properties. Red light can switch the chromophore into the Pfr state, which absorbs far-red light. Pfr undergoes thermal relaxation to the Pr state in the dark, but it can also be switched back by illumination with red light. Some bacterial phytochromes have an inverted dark reversion, with Pfr being more stable than Pr.[15,16] When switching between the two states, the chromophore transitions between a sequence of intermediate states,[17] which are called Lumi-R and Meta-R for the Pr-to-Pfr transition and Lumi-F and Meta-F for the reverse reaction.

The majority of plant, fungal and bacterial phytochromes share a conserved photosensory module (PSM) that contains three domains: PAS, GAF and PHY (Per/Arnt/Sim, cyclic guanosine monophosphate phosphodiesterase/adenyl cyclase/FhlA, and phytochrome-specific, respectively). Plant phytochromes

‡ Contributed equally
[a] *Department of Biological and Environmental Sciences, Nanoscience Center, University of Jyväskylä, PO Box 35, FI-40014 University of Jyväskylä, Finland.*
[b] *Department of Chemistry and Molecular Biology, Biochemistry and Biophysics, University of Gothenburg, PO Box 462, SE-40530 Gothenburg, Sweden.*
[c] *University of Helsinki, Faculty of Medicine, Anatomy, PO Box 63, FI-00014 University of Helsinki, Finland.*
* corresponding authors: westenho@chem.gu.se, janne.ihalainen@jyu.fi

have a partially unstructured N-terminal extension,[18] which is important for signaling.[19] All phytochromes have C-terminal output domains, which differ between different species. Plant phytochromes typically carry two PAS domains and a kinase-like domain, whose functional role is still debated. Many bacterial phytochromes have histidine kinase output domains and act as the first part of a two-component signaling system,[20] but other output domains also occur.[21,22] The bilin chromophore is covalently attached to a cystein in the PAS or GAF domain and it is typically inserted into the folded protein matrix with non-covalent links to all three domains (PAS, GAF, and PHY) of the PSM.

The discovery of bacterial homologs of phytochromes[2–5] marked a turning point in the field, because it has since then become possible to determine high-resolution structures of cyanobacterial and bacterial phytochromes.[17,23–35] Conserved amino acids in the vicinity of the chromophore are of special interest, because they are expected to guide the signal transduction from the chromophore to the protein. However, despite the availability of the crystal structures, comprehensive spectroscopic investigations of a large number of single-site mutants[36,37] and successful engineering of phytochromes into fluorescent proteins,[38–40] the functional role of the residues flanking the biliverdin remains scarcely understood.

Here, we investigate histidine 290 in the phytochrome from *Deinococcus radiodurans* (*Dr*P). Histidine 290 is widely conserved across the phytochrome superfamily. Some phytochromes in myxobacteria lack this histidine, but only when there are two phytochrome variants present in the same bacterium[41,42]. As such, the histidine must have an important role to play for the function of phytochromes. In Pr, the histidine residue is located at hydrogen bonding distance (2.7 Å) to the D-ring carbonyl and coordinates the D-ring directly[25,43] and through a water molecule.[24,44] It can therefore be expected to play a role in stabilizing the out-of-plane rotation of the D-ring with respect to the B- and C-rings. The residue has also been implicated in the isomerization reaction.[45] In Pfr, the D-ring carbonyl is facing away from the histidine and the histidine coordinates the propionic side chain of ring C instead.[43,46,47]

We compared the *Dr*P to the phytochrome 1 from the myxobacterium *Stigmatella aurantiaca* (*Sa*P1). *Sa*P1 is interesting, because the said histidine is naturally exchanged for a threonine.[41,42] The available crystal structure of $Sa\text{P1}_{PASGAF}$ indicated that the D-ring of the chromophore is not coordinated by the threonine directly.[41] Interestingly, *Sa*P1 has a higher Lumi-R quantum yield compared to other bacteriophytochromes. These observations were interpreted to mean that the absence of the histidine makes it easier for the D-ring to isomerize.[41] The suggestion is in line with a trend which had been observed earlier for the phytochromes 2 and 3 from *Rhodopseudomonas palustris*, which differ in the number of hydrogen bonds to the D-ring.[48,49]

However, under continuous red-light illumination, *Sa*P1 has an attenuated far-red absorption compared to prototypical bacteriophytochromes such as *Dr*P, similar to the H290N and H290Q mutants of *Dr*P.[36] This may be due to incomplete or inefficient photoconversion from Pr to Pfr, or due to changes in the shape and position of the Pfr spectra.[41,42] All of these samples have intact Pr spectra.

In order to investigate the role of H290 further, we use vibrational spectroscopy. The technique can give valuable information about the chemical environment of functional groups. In phytochromes, it has for example revealed that protonation events are important for the Pfr-to-Pr transition.[36,50,51] Time-resolved Fourier transform infrared (FTIR) absorption spectroscopy and FTIR spectra of cryo-trapped intermediates have revealed that the structural differences increase throughout the photocycle.[52,53] In agreement with crystal structures of the $Dr\text{P}_{PSM}$, which showed that parts of the PHY domain refolds in the transition from Pr to Pfr,[27] a set of peaks was identified in difference FTIR spectra (Pfr−Pr), which reflected these secondary structural changes.[54]

However, a general difficulty of protein vibrational spectroscopy is the assignment of spectral features to specific sites in the protein, limiting the structural insight that can be derived from the spectra. Luckily, the carbonyl groups of the D- and A-ring of the biliverdin chromophore can be clearly identified in Pfr−Pr difference spectra close to 1710 cm^{-1} and 1730 cm^{-1}, respectively.[45,55,56] When an oxygen of the carbonyl group acts as hydrogen bond acceptor, the C=O bond is weakened and the vibrational frequency down-shifts.[57] Hydrogen bonding of the carbonyl oxygens is also evident in pronounced shifts when H_2O is exchanged to D_2O in the buffer. For the Pfrof the $Dr\text{P}_{PSM}$, the biliverdin carbonyl frequency is identified at 1686 cm^{-1} by apoprotein labeling indicating a rather strong carbonyl coordination.[58]

Here, we report steady state and time-resolved IR spectra of $Dr\text{P}_{PSM}$, $Sa\text{P1}_{PSM}$, and a H290T mutant of $Dr\text{P}_{PSM}$. By determining the hydrogen bond coordination of the D-ring from the IR spectra and by presenting a new crystal structure of the mutant $Dr\text{P(H290T)}_{PASGAF}$, we investigate the role of H290 in the binding pocket of phytochromes.

2 Experimental

The samples $Dr\text{P(H290T)}_{PASGAF}$ and $Dr\text{P(H290T)}_{PSM}$ were mutated from the wild-type fragments[23] with a QuikChange Lightning Multi Site-Directed Mutagenesis Kit (Agilent Technologies) and primer 5'(CCT GAT CGC CTG CAC CCA CCA GAC GCC CTA CG)3'. The samples $Dr\text{P}_{PSM}$, $Dr\text{P(H290T)}_{PSM}$, and $Dr\text{P(H290T)}_{PASGAF}$ were produced and purified as described previously.[27,59] $Sa\text{P1}_{PSM}$ proteins were produced using the same protocol, but for purification with size-exclusion chromatography buffer (10 mM Tris, 10 mM NaCl, pH 8.0) was used. Additionally, protease inhibitor was added before cell lysis. The buffer for $Dr\text{P}_{PSM}$ and $Dr\text{P}_{PASGAF}$ and mutated samples was (30 mM Tris, pH 8.0). D_2O buffer was prepared by adjusting the apparent pH (as measured by a standard glass electrode) of D_2O solutions to 8.0 by addition of undeuterated concentrated HCl (aq). This corresponds to a pD of 8.4.[60] To exchange the solvent of the proteins, the solution was (1) concentrated three times and diluted with the new buffer, (2) illuminated five times with 655 nm (5 min) and 785 nm (5 min) laser diodes (∼35 mW) at about 0.2 mM protein concentration, and (3) concentrated to about 0.4 mM. The purpose of the light treatment was to exchange otherwise inaccessible hydrogens to the solvent.

Circular dichroism was measured in a Jasco J-715 spectropolarimeter and the UV/Vis spectra were measured by a PerkinElmer Lambda 850 UV/Vis spectrometer with the samples with concentrations of 3.4 μM of *Dr*P$_{PSM}$ and 4.0 μM of *Sa*P1$_{PSM}$, giving absorbances of about 0.3 at 700 nm. In order to achieve the anticipated state, the samples were illuminated until UV/Vis spectra did not change upon further illumination (usually for 5 min) using the same laser diodes that were used for D_2O exchange.

The extent of red light induced isomerization was determined by urea denaturation at low pH.[61] In the urea-denatured state, the bilin chromophore, still covalently attached to the now unfolded protein, maintains the ZZZ or ZZE conformation it had in the folded state. Each conformation exhibits a distinct UV/Vis absorbance spectrum.[61] Immediately after illumination with laser diodes and subsequent UV/Vis measurement, denaturation was induced by mixing 300 μL of the phytochrome solution with 700 μL of 10 M urea pH 2.5. UV/Vis of the denatured samples was then measured. Under these conditions dark reversion to Pr is minimal, with less than 0.2% dark reversion occurring after 5 minutes.[62] Spectral standards corresponding to the ZZZ-urea and ZZE-urea conformation were made using the dark (after illumination with 785 nm light) and illuminated (after illumination with 655 nm light) absorbance spectra of *Dr*P$_{PSM}$ pH 8.0 assuming 70% photoconversion. These standards were then used for spectral decomposition of the absorbance spectrum (450 to 800 nm) of urea-denatured phytochrome samples to determine the relative amount of phytochrome in the ZZZ and ZZE conformation. Spectral decomposition was carried out using a 32-bit version of SPECTRALAB software.[63]

Steady-state FTIR spectra were measured by a Nicolet Magna-IR 760 spectrometer. The concentrations of the samples were about 2 mM in H_2O buffers, which were (30 mM Tris, pH 8.0) for *Dr*P$_{PSM}$ and *Dr*P(H290T)$_{PSM}$ and (10 mM Tris, 10 mM NaCl, pH 8.0) for *Sa*P1$_{PSM}$. The sample concentrations in D_2O buffer were about 0.8 mM for *Dr*P$_{PSM}$, or 1.5 mM for *Dr*P(H290T)$_{PSM}$ and *Sa*P1$_{PSM}$. The sample was placed between two calcium fluoride windows held together by grease. The proteins were switched between the Pr and Pfr states by illumination before each measurement with 20 laser pulses of 1 s in length, interspersed with 0.5-s pauses to allow for heat dissipation. Pr was converted into Pfr by a 671 nm laser with a fluence of 70 mW/cm^2. Pr was recovered using a laser at 751 nm and a fluence of 50 mW/cm^2. Repetitive illumination series were performed to ensure maximum photoconversion.

Transient IR spectra were measured by a previously described setup.[64,65] Briefly, the sample was pumped in a closed cycle where it was illuminated by a 780 nm LED (to switch all the protein to the Pr state, approximately 5 mW/cm^2) before flowing between calcium fluoride windows. The windows were separated by a teflon spacer of either 50 μm (*Dr*P(H290T)$_{PSM}$) or 80 μm (*Sa*P1$_{PSM}$ and *Dr*P$_{PSM}$).[66] In the cell, the sample was illuminated by probe laser pulses as a reference, then by both pump and probe laser pulses. The pump was red light pulses at 500 Hz (692 nm, 100 fs, 300 nJ, 300 μm diameter). The probe was mid-infrared light pulses at 1000 Hz (central wavelength 5900 nm, 150 fs, 150 μm diameter). The probe and reference beams were detected by an HgCdTe detector (Infrared Systems Development). Waterlines were used for the calibration of the spectral positions and to determine the spectral resolution (about 4 cm^{-1}). At long times (2.6 ns and above), spectra were measured repeatedly (at a number of closely spaced time points) in order to obtain the Lumi-R spectrum with a good signal-to-noise ratio. To minimize buffer absorption in the spectral window of interest, the samples were kept in D_2O buffer at concentrations of about 0.1 mM (*Sa*P1$_{PSM}$), 0.3 mM (*Dr*P$_{PSM}$) and 0.5 mM (*Dr*P(H290T)$_{PSM}$).

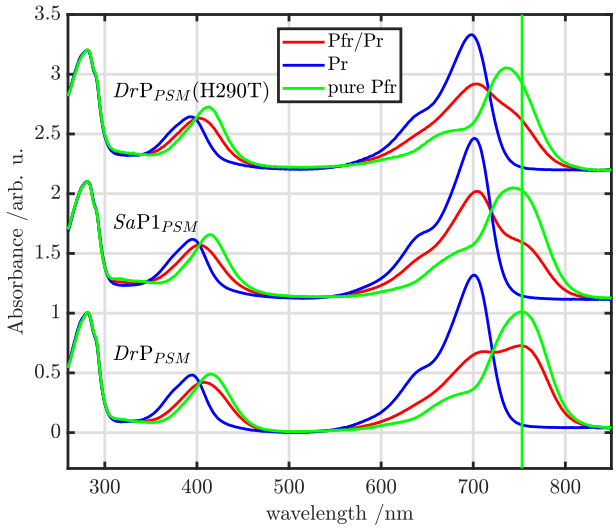

Fig. 1 UV/Vis absorption spectra of *Dr*P$_{PSM}$, *Sa*P1$_{PSM}$, and *Dr*P(H290T)$_{PSM}$ after 785 nm illumination (Pr state, blue curves) and after 655 nm illumination (Pfr/Pr photoequilibrium, red curves). The green spectra are reconstructed spectra of the Pfr state, as described in the main text. The line marks the peak of the Pfr absorption in *Dr*P$_{PSM}$.

Crystallization of *Dr*P(H290T)$_{PASGAF}$ was performed as previously described for the wild-type *Dr*P$_{PASGAF}$.[44] Protein with a concentration of 20 mg/ml was mixed with reservoir (67 mM sodium acetate pH 4.95, 3.3% PEG 400, 1 mM DTT, 30% 2-methyl-2,4-pentanediol) in a 1:1 ratio as hanging drops. Crystals formed in the course of hours and were flash-frozen in liquid nitrogen before data collection. The diffraction data was collected in beamline ID30A-3 at the European Synchrotron Radiation Facility (ESRF). The data was processed with the XDS program package version March 1, 2015.[67] Like the wild-type counterpart,[44] the crystals belonged to space group C121, except that two monomers were contained in the asymmetric unit. The structure was solved by molecular replacement with Phaser[68] with 5K5B[44] as the search model. Refinement was performed with REFMAC version 5.8.0135[69] by using automatic weights and anisotropic temperature factors. The model was built with Coot 0.8.2.[70] Statistics from data collection and refinement can be found in Table 1. The final structure had Ramachandran statistics of 98.0% in preferred regions, 2.0% in allowed regions, and 0% outliers.

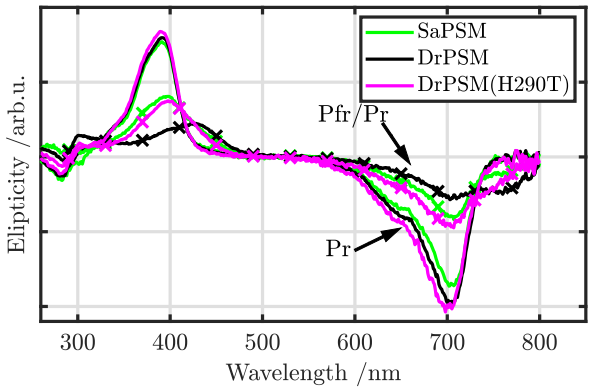

Fig. 2 CD spectra of the *Dr*P$_{PSM}$, *Sa*P1$_{PSM}$, and *Dr*P(H290T)$_{PSM}$ after 785 nm illumination (the Pr state) and after 655 nm illumination (the Pfr/Pr photoequilibrium). "x" marks the Pfr/Pr spectra.

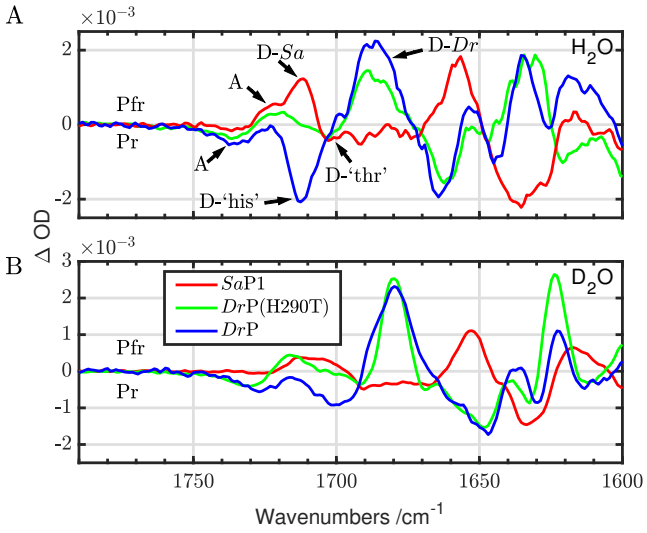

Fig. 3 FTIR difference spectra between Pr (negative) and Pfr (positive) states of *Dr*P$_{PSM}$, *Dr*P(H290T)$_{PSM}$ and *Sa*P1$_{PSM}$ are shown in H_2O (top) and D_2O (bottom). The arrows indicate the assigned peak position of the carbonyl peaks (see text for details).

3 Results

3.1 Steady-state spectroscopy

Fig. 1 shows the UV/Vis absorption spectra of *Dr*P$_{PSM}$, *Dr*P(H290T)$_{PSM}$, and *Sa*P1$_{PSM}$. The absorption spectra in Pr are highly similar for the three samples, but differ after illumination with 655 nm light. This effect can be reverted by reintroducing a histidine instead of the unusual threonine into *Sa*P1.[42]

To investigate this issue, we determined the amount of isomerized biliverdin in the Pr/Pfr photoequilibrium spectroscopically after denaturation of the protein with urea. Assuming that the Pfr/Pr equilibrium (r) for *Dr*P$_{PSM}$ was 30%,[27] we found that the amount of chromophore in ZZZ conformation (corresponding to Pr) in the Pfr/Pr equilibrium was 44% in *Dr*P(H290T)$_{PSM}$, and 49% in *Sa*P1$_{PSM}$. With this data we estimated the pure Pfr spectrum of the proteins as $I_{Pfr} = (I_{Pfr} - r * I_{Pr})/(1-r)$ (see Fig. 1). The Pfr spectra of the proteins which lack the histidine are blueshifted by 10 nm (*Sa*P1$_{PSM}$) and 15 nm (*Dr*P(H290T)$_{PSM}$) compared to *Dr*P$_{PSM}$. This blue shift means that the histidine-less proteins have a higher differential Pfr/Pr absorption compared to *Dr*P$_{PSM}$ at the excitation wavelength (655 nm). This in turn causes the photoequilibrium to shift towards Pr and results in a smaller concentration of Pfr in the photoequilibrium. These effects quantitatively explain the "non-prototypical" shapes of the Pfr/Pr spectra of *Dr*P(H290T)$_{PSM}$ and *Sa*P1$_{PSM}$ (Fig. 1).

Fig. 2 shows the circular dichroism (CD) of the chromophore absorption. We find that the CD signals of the three samples in Pr are similar, except for a small difference in intensity at the main absorption band at 700 nm. This indicates that the overall conformation of the biliverdin is similar, which is confirmed when comparing the crystal structures of *Sa*P1$_{PSM}$ and *Dr*P$_{PSM}$ (structures not shown) and *Dr*P(H290T)$_{PASGAF}$ and *Dr*P$_{PASGAF}$ (Fig. 6). The CD spectra under illumination appear to be different. This is predominantly an effect of the different concentrations of Pr and Pfr in the photoequilibrium.

Fig. 3 shows the FTIR difference spectra (Pfr minus Pr). A series of peaks is observed in the carbonyl region of 1670–1750 cm^{-1}. In H_2O (D_2O), *Dr*P$_{PSM}$ has negative peaks at 1737 (1728) cm^{-1} and 1713 (1701) cm^{-1}, and a positive peak at 1686 (1680) cm^{-1}. There is even a small positive peak at 1723 (1716) cm^{-1} in *Dr*P$_{PSM}$, but it overlaps with the negative 1713 cm^{-1} peak. For *Sa*P1$_{PSM}$, only one negative peak at 1733 (1729) cm^{-1} is clearly visible in the relevant range, along with a broad, but distinct negative band between 1703 (1691) cm^{-1} and 1674 (1667) cm^{-1}. Two positive peaks are found at 1722 (1713) cm^{-1} and 1712 (1707) cm^{-1}. For *Dr*P(H290T)$_{PSM}$, the negative peaks are at similar frequencies as for *Sa*P1$_{PSM}$ at 1737 (1731) cm^{-1} and at 1703 (1691) cm^{-1} and the positive peaks resemble the positions in the wild-type *Dr*P$_{PSM}$ at 1719 (1716) cm^{-1} and 1689 (1680) cm^{-1}.

We assign the A-ring carbonyl (Pr) to the negative peaks at 1737 cm^{-1} (*Dr*P$_{PSM}$) and 1733 cm^{-1} (*Sa*P1$_{PSM}$) in accordance with Ref.[55], assigned using specific isotope labeling of the chromophore. The assignment is supported by the fact that the peak is unperturbed in *Dr*P(H290T)$_{PSM}$ by the H290T mutation, which is not in the proximity of the A ring. Since the A ring does not isomerize and only moves moderately between the Pr and Pfr states,[46] only moderate shifts of the vibrational frequency are expected for the A-ring carbonyl. We therefore assign the positive peaks at 1722 cm^{-1} (*Sa*P1$_{PSM}$), 1719 cm^{-1} (*Dr*P(H290T)$_{PSM}$), and 1723 cm^{-1} (*Dr*P$_{PSM}$) to the A ring. In summary, the position of the infrared peak of the A-ring carbonyl shifts moderately to lower frequencies after photoconversion from Pr to Pfr in all investigated samples and it does not depend on the presence of H290.

In contrast, the position of the D-ring carbonyl depends on the presence of H290 in Pr, but not in Pfr. The negative peak at 1712 cm^{-1} for *Dr*P$_{PSM}$ is not observed for *Dr*P(H290T)$_{PSM}$ and *Sa*P1$_{PSM}$, where H290 is missing. Instead, a red-shifted peak is observed in both proteins at about 1703 cm^{-1}. The positive peak at 1686 cm^{-1} is common to *Dr*P$_{PSM}$ wildtype and the mutant, which indicates that H290 does not directly interact with the

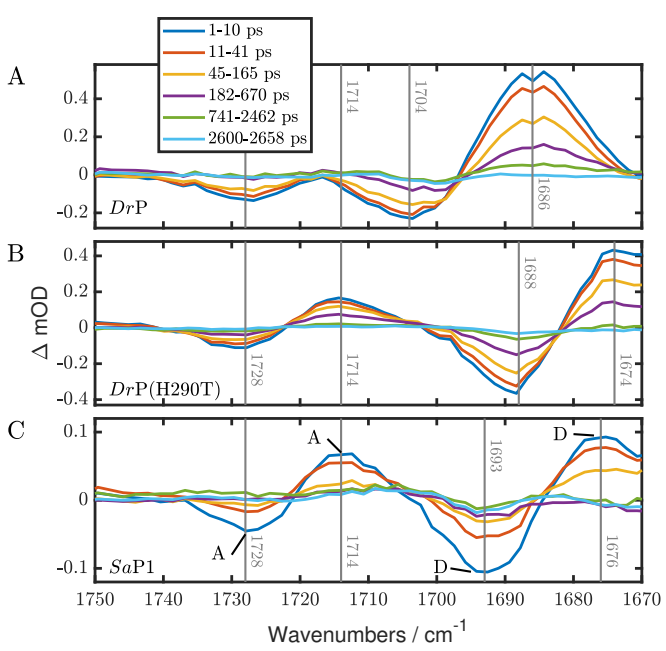

Fig. 4 Time-averaged transient IR spectra of the biliverdin carbonyl region of DrP_{PSM}, $DrP(H290T)_{PSM}$, and $SaP1_{PSM}$, all in D_2O. The frequencies of the A and D-ring absorptions are indicated as grey lines.

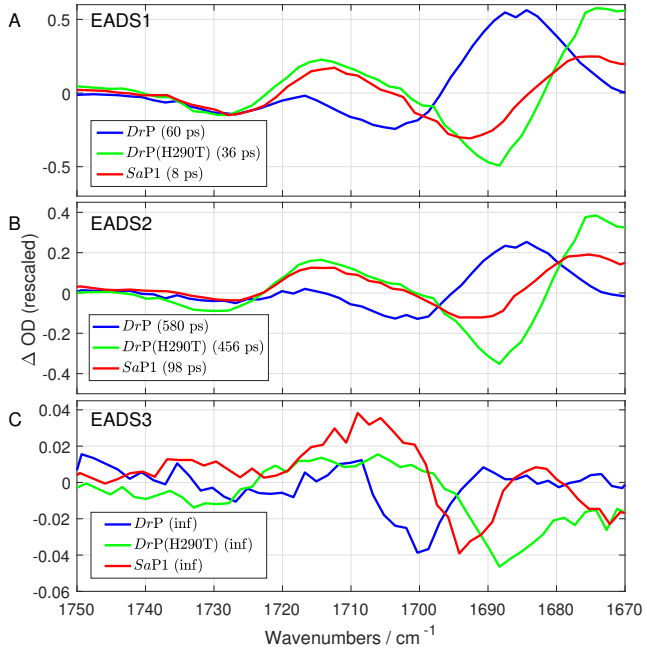

Fig. 5 Evolution-associated difference spectra (EADS) of DrP_{PSM}, $DrP(H290T)_{PSM}$, and $SaP1_{PSM}$. The EADS were obtained by global analysis with the glotaran software package.[71] The decay of the excited state was fit with 2 components (EADS1 and EADS2), for the third time constant which corresponds to the lifetime of the Lumi-R state was fixed to 100 ns, since it lies outside of the experimental time window.

D-ring carbonyl in Pfr.[58] This is consistent with the available crystal structures for Pfr.[26,46] In $SaP1_{PSM}$, the positive (Pfr) peak for the D-ring carbonyl appears up-shifted by 26 cm^{-1} at 1712 cm^{-1} compared to the *Dr*P phytochromes, at a spectral position similar to the PSM from a plant phytochrome.[55] The difference in spectral position in Pfr reflects a different coordination of the D-ring carbonyl in the Pfr state. The most likely candidate is the presence of H201 (*Dr*P numbering), which is only present in *Dr*P, not in *Sa*P1, and which is located very close to the D-ring carbonyl in one of the monomers resolved in the Pfr-state crystal structure of DrP_{PSM}.[46]

3.2 Transient-IR spectroscopy

In order to further verify the spectral position of the D-ring carbonyl peaks in Pr, we also measured infrared absorption spectra on pico- and nanosecond time scales (Fig. 4). In these data, negative features are again due to the bleach of Pr absorptions, but the positive features are due to photoinduced absorption of the excited and intermediate states.

The transient IR spectra in the 1670–1750 cm^{-1} range in D_2O reveal that all samples have a negative peak at approximately 1728 cm^{-1}. A corresponding positive peak appears at 1714 cm^{-1}. In accordance with the FTIR spectra, we assign these peaks to the A-ring carbonyl. For DrP_{PSM}, the peak at 1714 cm^{-1} is not visible, but the comparison with the data of $DrP(H290T)_{PSM}$ and $SaP1_{PSM}$ indicates that a peak at the same position could be present but overlaps with the bleach at 1704 cm^{-1}.

At lower wavenumbers, the peak positions vary with the presence of the histidine. Negative peaks are found at 1688 cm^{-1} and 1693 cm^{-1} for $DrP(H290T)_{PSM}$ (panel b) and $SaP1_{PSM}$ (panel c), respectively, while the corresponding negative peak is found at 1704 cm^{-1} for DrP_{PSM}. The positive peaks follow the same pattern and are located at 1676 cm^{-1} ($SaP1_{PSM}$), 1674 cm^{-1} ($DrP(H290T)_{PSM}$) and 1686 cm^{-1} (DrP_{PSM}). These peaks are assigned to the D-ring carbonyl.

Compared to the FTIR difference spectra (Pfr−Pr), the peak positions can be more clearly identified, because the overlapping Pfr absorption is missing. Importantly, the data confirm that the absorption of the D-ring carbonyl in the Pr-state down-shifts by 10 cm^{-1} ($SaP1_{PSM}$) and 15 cm^{-1} ($DrP(H290T)_{PSM}$) when the histidine is exchanged to the threonine. This shift could be due to a change in the coordination of the chemical group, or due to an alteration of the conjugation in the D-ring. We consider the latter possibility to be much less likely, because of the highly similar UV/Vis absorption and CD spectra of *Dr*P and *Sa*P1 in the Pr state. The former possibility is supported by a comparison between the peak position in H_2O (Fig. 3) and D_2O (Fig. 4). It is revealed that the D-ring carbonyl absorptions shift by approximately 10 cm^{-1} due to the H–D exchange (with some variation between samples depending on spectral position and shape), which indicates that hydrogen coordination controls the vibrational frequencies. Assignment of the shifts to a change in the coordination of the D-ring carbonyl also follows Toh *et al.*, who used the same interpretation for IR spectroscopic analysis of two other phytochromes.[49] Combined, the findings strongly suggests that the coordination of the D-ring carbonyl by the hydrogen bonding partners in Pr is tighter when the histidine is missing.

Our transient infrared absorption data of the proteins covered

Table 1 Decay times (τ) and amplitudes of EADS (A) of the three components in the global analysis

component	*Dr*P$_{PSM}$ τ	A*	*Dr*P(H290T)$_{PSM}$ τ	A*	*Sa*P1$_{PSM}$ τ	A*
1	60 ps	1	36 ps	1	8 ps	1
2	580 ps	0.40	456 ps	0.66	98 ps	0.59
3	non-dec.**	0.05	non-dec.**	0.07	non-dec.**	0.12
τ_{ave}***	260 ps		298 ps		51 ps	

* A was estimated by integrating the EADS over the detected spectral range; the estimated confidence range for A is ±20%.
** The lifetime of the non-decaying component τ_3 was fixed to 100 ns.
*** τ_{ave} is the average decay time computed from the DADS (see supplementary information, table SI 1).

a time range up to 2.6 nanoseconds, which covers the decay of the excited state and the Lumi-R formation. The decay profiles at characteristic spectral regions indicate that the excited state decay profile does not follow single-exponential behavior (Fig. SI 1), in line with a number of other ultrafast studies of bacteriophytochromes.[41,48,49,72,73] The data could be fitted satisfactorily by global analysis with a three-component sequential scheme (Fig. 5).[71] The characteristic lifetimes for each obtained evolution-associated difference spectrum (EADS) are tabulated in Table 1 and the EADS are shown in Fig. 5.

EADS1 and EADS2 are associated with the decay of the excited state. In each sample, small changes in the spectral profile between EADS1 and EADS2 can be observed (Fig. 5 and SI Fig. 2–4). In particular, in the case of *Dr*P$_{PSM}$, the negative band at 1704 cm^{-1} of EADS1 shifts to lower frequency in EADS2 (Fig. SI 2). The sample-specific differences in the spectral dynamics are as discussed above. Comparing the lifetimes obtained from global analysis is difficult, because they depend on the amplitudes of the corresponding spectra and the number of components used for the fits.[74] Therefore, we have calculated average lifetimes. For this, we have calculated the amplitudes of the corresponding decay-associated spectra (DADS) of each component over the detected spectral range (Table SI 1 and Fig. SI 5). Similarly to the raw decay curves (Fig. SI 1), the averaged lifetimes indicate that the decay of the excited state is faster for *Sa*P1$_{PSM}$ ($\tau_{ave} = 51$ ps) than for *Dr*P$_{PSM}$ (260 ps) and *Dr*P(H290T)$_{PSM}$ (298 ps).

EADS3 represents Lumi-R and overlaps well with the spectra recorded at 2.6 ns (Fig. 4, 5, and SI 2–4). All three samples show a broad positive feature over the spectral range from 1720 cm^{-1} to 1680 cm^{-1} partially overlapped with the bleach from the D-ring carbonyl, whose position is different for each studied sample. The quantum yield of Lumi-R is estimated from the spectral amplitudes of the EADS3. For the estimation of the yield, it was assumed that the oscillator strength does not change between the excited state and Lumi-R. Since the infrared bands are overlapping in the spectra, we consider that the quoted amplitudes have a confidence interval of ±20%. Thus, we find that, compared to *Dr*P$_{PSM}$, the Lumi-R yield is significantly higher for *Sa*P1$_{PSM}$[41]. Consistent with higher Lumi-R yield the excited state decay is faster for *Sa*P1$_{PSM}$than for *Dr*P$_{PSM}$. However, the decay time of the *Dr*P(H290T)$_{PSM}$is slightly slower than the wild type whereas the Lumi-R yield is slightly higher (Tab. 1 and Fig. SI 1). In summary, we conclude that the exchange of His290 for Thr indeed changes the coordination of the D-ring C=O group, but that this does not necessarily lead to a higher Lumi-R yield and faster decay time when comparing *Dr*P(H290T)$_{PSM}$ to *Dr*P$_{PSM}$.

3.3 Crystallography

Table 2 X-ray diffraction data collection and refinement statistics

Parameter	PAS-GAF-H290T
Data collection[a]	
Space group	C121
Cell dimensions	
a,*b*,*c* (Å)	94.8, 53.0, 135.9
α, β, γ (°)	90.0, 93.3, 90.0
Resolution (Å)	47.3–1.40 (1.44–1.40)
R_{Meas}	0.124 (1.552)
$CC_{1/2}$	0.997 (0.336)
I/σ(I)	7.48 (0.93)
Completeness (%)	99.7 (99.5)
Redundancy	4.25 (4.26)
Wilson B-factor	16.6
Refinement	
Resolution (Å)	47.3–1.40 (1.44–1.40)
No. of reflections	125,781(9,227)
R_{work}/R_{free}	0.148/0.198[b] (0.4111/0.423)
Overall B-factor	24.0
No. of atoms	5741
Protein[c]	4790
Ligand[d]	126
Water	573
Geometry	
RMSD	
Bond lengths (Å)	0.028
Bond angles (°)	2.55
Ramachandran	
Favored (%)	98.0
Allowed (%)	2.0
Outliers (%)	0
PDB Code	6FTD

[a] Outer shell values are in parenthesis.
[b] Test set for R_{Free} calculation constitutes 5%.
[c] Two protein molecules in asymmetric unit.
[d] Includes atoms from two biliverdins, six acetates and two (4*S*)-methyl-2,4-pentanediols.

The conclusion that the D-ring carbonyl is coordinated more strongly when histidine 290 is exchanged to a threonine is in disagreement with the crystal structure of *Sa*P1 at 2.73 Å resolution. The structure indicated that the threonine is too far from the D-ring carbonyl to coordinate it, which was seemingly in line with the high Lumi-R yield of the *Sa*P1$_{PSM}$.[41] In order to structurally underpin the spectroscopic findings, we solved the crystal structure of *Dr*P(H290T)$_{PASGAF}$ at 1.4 Å resolution. The mutation mimics of the naturally occurring mutation in *Sa*P1. *Dr*P(H290T)$_{PASGAF}$ crystallized as monomers in the same crystallization conditions as *Dr*P$_{PASGAF}$.[44]

The overall structure and fold of the two proteins is very similar (RMSD = 0.2 Å). The *Dr*P(H290T)$_{PASGAF}$ crystals had an elongated asymmetric unit that contained two monomers instead of one monomer in the *Dr*P$_{PASGAF}$ crystal.[44] This is caused by pseudo-translation, which is a crystallographic artifact where a fraction (here 25.3%) of two highly similar copies of the proteins are slightly displaced in relation to each other. Due to this displacement, a larger asymmetric unit is detected, which encloses the two highly similar monomers. Here, this leads to

additional electron density in monomer B, which could not be modeled (around residues 59–67), but it did not affect the structure of monomer A. The effect explained the *R*-factors and the R_{work}/R_{free} gap (0.148/0.198) of the final refinement, which are acceptable but slightly higher than expected for a structure at 1.4 Å resolution.

Compared to *Dr*P$_{PASGAF}$, the D ring of *Dr*P(H290T)$_{PASGAF}$ biliverdin was slightly more tilted relative to the rings B and C and repositioned closer to the 290 residue (Fig. 6a). We obtained distinct electron density features in the vicinity of the chromophore, which we assign as water molecules. Fig. 6b shows the hydrogen bonding network for the wild-type *Dr*P$_{PASGAF}$, which involves the D-ring carbonyl and H290 together with two highly coordinated waters (W1 and W2) that reside between the D-ring carbonyl and the C-ring propionate. In Figure 6c it is shown that the space between the D-ring and T290 allows access for two additional waters (W3 and W4) in H-bonding distance to the D-ring carbonyl. The density for W4 is more clearly observed in monomer A compared to monomer B, which is probably due to the crystallographic pseudo-translation effect (see above).

The electron density for W3 and W4 is weaker than for W1 and W2, indicating that they are disordered in the structure, have low occupancy, or are only transiently present. Figure 6d shows electron density for a composite omit map with the waters W1–4 removed from the model. The densities in the omit maps are strong for W1 and W2, and weaker and anisotropic for W3 and W4, but confirm their presence in H-bonding distance to the D-ring carbonyl. When refined, the distance between W3 and W4 (2.5 Å) is too small for normal hydrogen bonding. The observed density is either consistent with two waters, which have correlated positions and occupancies, or with the presence of an $H_3O_2^-$ or $H_5O_2^+$ cluster. For both clusters, a distance of 2.5 Å is expected between the 2 oxygen atoms. Furthermore, there is extra electron density present next to the W3 water that is prolonged towards the surface of the protein, as demonstrated in Fig. 6e. This forms a potential water channel that might account for the weaker defined density of the waters and their high degree of disorder. Figure 6f shows how this electron density fits into a pore in the protein surface and indicate that W3 and W4 can be exchanged with the solvent through this water channel.

The crystallographic data of *Dr*P(H290T)$_{PASGAF}$ indicate that the D-ring carbonyl can be coordinated by three hydrogen bonds. In *Dr*P$_{PASGAF}$, the carbonyl is only coordinated twice: by one of the waters and the NE-H group of H290 (Fig. 6a). Furthermore, the D-ring in *Dr*P(H290T)$_{PASGAF}$ is slightly repositioned closer to W2 compared to *Dr*P$_{PSM}$, which should strengthen the interactions with the hydrogen bonding partners. Thus, waters fill the void created by replacement of H290 by threonine and these waters coordinate the carbonyl group. This underpins the conclusions from the infrared spectra, which indicated a tighter coordination of the D-ring carbonyl of the *Dr*P(H290T)$_{PSM}$ compared to *Dr*P$_{PSM}$.

Although we analyze the structures of *Dr*P(H290T)$_{PASGAF}$ in Fig. 6, the similarity of the negative (Pr) peaks in the infrared spectra for *Sa*P1$_{PSM}$ and *Dr*P(H290T)$_{PSM}$ suggests that the structure around the D-ring carbonyl in *Sa*P1$_{PSM}$ is similar. In the pre-

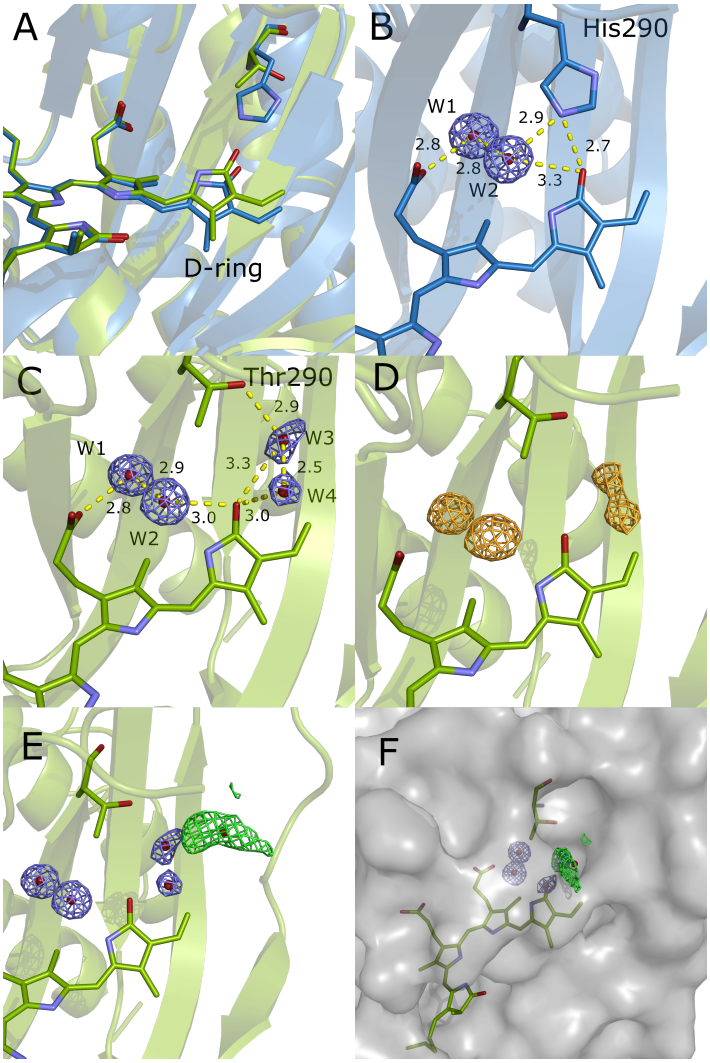

Fig. 6 Structural comparison of the Pr structures of *Dr*P(H290T)$_{PASGAF}$ (green) and wild-type *Dr*P$_{PASGAF}$ (blue, PDB ID; 5K5B). A) The impact of the mutation on the D ring of the chromophore. As an effect of the histidine removal, the D ring is slightly repositioned towards the 290 residue. B) The waters (W1–2) and hydrogen bonding network around the D-ring carbonyl in *Dr*P$_{PASGAF}$. Electron density around the waters is shown at 1.5 RMSD and hydrogen bond lengths are shown in Angstroms. C) The waters (W1–4) and hydrogen bonding network around the D-ring carbonyl in *Dr*P(H290T)$_{PASGAF}$. Electron density around the waters is shown at 1.0 RMSD and hydrogen bond lengths are shown in Angstroms. D) Electron density for the waters (W1–4) in *Dr*P(H290T)$_{PASGAF}$ as obtained from a composite omit map. The composite omit map was calculated by Phenix (version 1.13-2998) with default settings and omitting waters W1–4. The electron density (orange) is shown at 1.0 RMSD. E) Elongated difference electron density (green) shown for a water in H-bonding distance to W3. The density extends out to the surface of the protein indicating the existence of a water channel. Electron density for waters is shown at 1.0 RMSD and difference density is shown at 3.5 RMSD. F) The surface of the protein and the pore with the difference electron density inserted in to the pore. Densities shown as in E.

viously published structure of *Sa*P1$_{PASGAF}$, waters were not modeled around the D-ring carbonyl, presumably due to low resolution (2.7 Å), but our spectroscopic and structural data indicates that waters should be present to coordinate the D-ring. *Sa*P1$_{PSM}$ may also form interactions with a serine residue (287),[41] but the position of this residue does not hinder the presence of additional waters.

4 Discussion

The mechanism of photoisomerization in phytochromes has been debated. In one model, photoisomerization occurs within femtoseconds,[75] but other evidence suggest that the ring rotation occurs on a timescale of tens of picoseconds.[45,48,76] The relatively tight coordination of the D-ring carbonyl that we find in this study is consistent with the latter model as several hydrogen bonds have to be broken between the carbonyl and its binding partners before isomerization can occur.

Our data (Fig. 5) indicate that *Sa*P1$_{PSM}$ and *Dr*P(H290T)$_{PSM}$, which lack H290, have a tighter coordination of the D-ring carbonyl than *Dr*P$_{PSM}$. However, the Lumi-R quantum yield and excited-state decay times do not correlate with this binding pattern, as the yield is higher for *Sa*P1$_{PSM}$ and similar for *Dr*P(H290T)$_{PSM}$, compared to *Dr*P$_{PSM}$ (see Table 1). Thus, the data do not fall into the trend that would be suggested by the model which has derived from data for the phytochrome 2 and 3 of *R. palustris* (*Rp*P2/3).[48,49] According to the model, the excited-state decay time should increase and the Lumi-R quantum yield should decrease with increasing H-bonding to the D ring.

In order to explain this discrepancy, we consider two possibilities. Firstly, it cannot be completely excluded that either our or the reported[48,49] correlations between hydrogen bonding around the D-ring carbonyl and the Lumi-R quantum yield are coincidental. It may be that other structural effects mask the effects of the hydrogen bonding network to the D-ring. This may reflect that the initial photoreaction in phytochromes involves more than just the H290 and appears to be collective in nature. This, for example, is in line with the fact that many mutations close to the chromophore hinder but do not inhibit the photoconversion[36] and that several point mutations, but not the H290, are necessary to turn phytochromes into fluorescent proteins.[38–40,49] Secondly, the discrepancy in interpretation may be explained by the nature of the hydrogen bonding partners. In the present case, the additional hydrogen bonds for *Dr*P(H290T)$_{PASGAF}$ (and presumably also for *Sa*P1$_{PSM}$) are to water molecules, whereas the earlier reported *Rp*P3 phytochrome has additional hydrogen bonds to amino acid side chains.[48,77] Waters are highly mobile and may be dragged along with a rotating D-ring, whereas amino acid side chains are more tightly anchored in the protein structure. Thus, the hydrogen bonding network around the D-ring carbonyl of *Rp*P3 may be more restrictive than the networks in *Dr*P(H290T) and in *Sa*P1.

In any case, our structure of *Dr*P(H290T)$_{PASGAF}$ indicates electron density for 4 waters (or 2 waters and a cluster formed out of two waters). This highlights that waters are an integral part of the pocket in phytochromes. Water molecules may act as a lubricant around the D-ring, holding it in place, but also providing it with sufficient freedom to isomerize. Apparently, both the histidine and the threonine in position 290 can establish a water network, which stabilizes the Pr state, but which also enables formation of the Lumi-R state.

Considering the wide conservation of the investigated histidine, it must play a essential role. The crystal structures of *Dr*P$_{PSM}$ in the Pfr state[27,46] show that H290 coordinates the propionics of the C-ring. An unusual back-reaction channel has been identified for the *Sa*P1$_{PSM}$ from Lumi-R to Pr,[41] which may be related to the fact that the propionic of the C-ring cannot find a coordination partner in the absence of H290. Even though the propionic side chain is not connected to the light-absorbing π-system, removal of the histidine may alter the overall arrangement of the chromophore in Pfr. This is evident in the blue-shifted Pfr spectra of the histidine-less samples, leading to a shift in photoequilibrium (Fig. 1). We note that this effect is likely to be functionally relevant, since the Pr/Pfr ratio under constant light determines the biochemical activity of the protein.

5 Conclusion

Here, we present crystallographic and spectroscopic evidence that the D-ring carbonyl in phytochromes is coordinated by waters and that this coordination strength is increased when the conserved histidine 290 is exchanged into a threonine. Awaiting structures of the excited or intermediate states of phytochromes, spectroscopic and comparative studies between different phytochromes will continue to be important to illuminate the role of the residues flanking the bilin chromophore. The water cluster revealed by our new crystal structure deserves further attention, for example by quantum-chemical modeling. It would also be important to detect the position and presence of hydrogen atoms. Our study underpins that water molecules which embed the chromophore into the protein binding pocket are integral parts of the phytochrome machinery for signal transduction.

6 Acknowledgements

We thank Alli Liukkonen for protein production, Emina Stojković, Richard Vierstra and Katrina Forest for the original plasmids, Pasi Myllyperkiö and Satu Mustalahti for help with the transient IR setup, and Valentyna Kuznetsova for help with the global analysis. The work was funded by the Bengt Lundqvist Memorial Foundation (N.L.), the Swiss National Science Foundation (P2ZHP2_164991 to B.S.B.), and the Academy of Finland grants 296135 to J.A.I. and 285461 to H.T. S.W. acknowledges the European Research Council for funding. The atomic coordinates and structure factors of *Dr*P(H290T)$_{PASGAF}$ have been deposited in the Protein Data Bank (http://wwpdb.org/) with code 6FTD.

References

1 W. L. Butler, K. H. Norris, H. W. Siegelman and S. B. Hendricks, *Proc. Natl. Acad. Sci. U.S.A.*, 1959, **45**, 1703–1708.

2 D. M. Kehoe and A. R. Grossman, *Science*, 1996, **273**, 1409–1412.

3 K. C. Yeh, S. H. Wu, J. T. Murphy and J. C. Lagarias, *Science*, 1997, **277**, 1505–1508.

4 J. Hughes, T. Lamparter, F. Mittmann, E. Hartmann, W. Gartner, A. Wilde and T. Borner, *Nature*, 1997, **386**, 663.

5 S. J. Davis, A. V. Vener and R. D. Vierstra, *Science*, 1999, **286**, 2517–2520.

6 S. H. Bhoo, S. J. Davis, J. Walker, B. Karniol and R. D. Vierstra, *Nature*, 2001, **414**, 776–779.

7 A. Blumenstein, K. Vienken, R. Tasler, J. Purschwitz, D. Veith, N. Frankenberg-Dinkel and R. Fischer, *Curr. Biol.*, 2005, **15**, 1833–1838.

8 G. Bae and G. Choi, *Annu. Rev. Plant Biol.*, 2008, **59**, 281–311.

9 K. A. Franklin and P. H. Quail, *J. Exp. Bot.*, 2010, **61**, 11–24.

10 M. Legris, C. Klose, E. S. Burgie, C. C. R. Rojas, M. Neme, A. Hiltbrunner, P. A. Wigge, E. Schäfer, R. D. Vierstra and J. J. Casal, *Science*, 2016, **354**, 897–900.

11 N. C. Rockwell, D. Duanmu, S. S. Martin, C. Bachy, D. C. Price, D. Bhattacharya, A. Z. Worden and J. C. Lagarias, *Proc. Natl. Acad. Sci. U.S.A.*, 2014, **111**, 3871–3876.

12 C. Song, T. Rohmer, M. Tiersch, J. Zaanen, J. Hughes and J. Matysik, *Photochem. Photobiol.*, 2013, **89**, 259–273.

13 X. J. Yang, Z. Ren, J. Kuk and K. Moffat, *Nature*, 2011, **479**, 428–U190.

14 H. Linschitz and V. Kasche, *J. Biol. Chem.*, 1966, **241**, 3395–3403.

15 B. Karniol and R. D. Vierstra, *Proc. Natl. Acad. Sci. U.S.A.*, 2003, **100**, 2807–2812.

16 T. Lamparter, M. Carrascal, N. Michael, E. Martinez, G. Rottwinkel and J. Abian, *Biochem.*, 2004, **43**, 3659–3669.

17 A. Björling, O. Berntsson, H. Lehtivuori, H. Takala, A. J. Hughes, M. Panman, M. Hoernke, S. Niebling, L. Henry, R. Henning, I. Kosheleva, V. Chukharev, N. V. Tkachenko, A. Menzel, G. Newby, D. Khakhulin, M. Wulff, J. A. Ihalainen and S. Westenhoff, *Sci. Adv.*, 2016, **2**, e1600920.

18 S. von Horsten, S. Straß, N. Hellwig, V. Gruth, R. Klasen, A. Mielcarek, U. Linne, N. Morgner and L.-O. Essen, *Sci. Rep.*, 2016, **6**, 34366.

19 J. R. Cherry, D. Hondred, J. M. Walker and R. D. Vierstra, *Proc. Natl. Acad. Sci. U.S.A.*, 1992, **89**, 5039–5043.

20 M. E. Auldridge and K. T. Forest, *Crit. Rev. Biochem. Mol. Biol.*, 2011, **46**, 67–88.

21 E. Giraud, J. Fardoux, N. Fourrier, L. Hannibal, B. Genty, P. Bouyer, B. Dreyfus and A. Verméglio, *Nature*, 2002, **417**, 202–205.

22 B. Karniol, J. R. Wagner, J. M. Walker and R. D. Vierstra, *Biochem. J.*, 2005, **392**, 103–116.

23 J. R. Wagner, J. S. Brunzelle, K. T. Forest and R. D. Vierstra, *Nature*, 2005, **438**, 325–331.

24 E. S. Burgie, T. Wang, A. N. Bussell, J. M. Walker, H. Li and R. D. Vierstra, *J. Biol. Chem.*, 2014, **289**, 24573–24587.

25 L. O. Essen, J. Mailliet and J. Hughes, *Proc. Natl. Acad. Sci. U.S.A.*, 2008, **105**, 14709–14714.

26 X. Yang, J. Kuk and K. Moffat, *Proc. Natl. Acad. Sci. U.S.A.*, 2008, **105**, 14715–14720.

27 H. Takala, A. Björling, O. Berntsson, H. Lehtivuori, S. Niebling, M. Hoernke, I. Kosheleva, R. Henning, A. Menzel, J. A. Ihalainen and S. Westenhoff, *Nature*, 2014, **509**, 245–248.

28 G. Gourinchas, S. Etzl, C. Göbl, U. Vide, T. Madl and A. Winkler, *Sci. Adv.*, 2017, **3**, e1602498.

29 L. H. Otero, S. Klinke, J. Rinaldi, F. Velázquez-Escobar, M. A. Mroginski, M. Fernández López, F. Malamud, A. A. Vojnov, P. Hildebrandt, F. A. Goldbaum and H. R. Bonomi, *J. Mol. Biol.*, 2016, **428**, 3702–3720.

30 S. Nagano, P. Scheerer, K. Zubow, N. Michael, K. Inomata, T. Lamparter and N. Krauß, *J. Biol. Chem.*, 2016, **291**, 20674–20691.

31 X. Yang, E. A. Stojković, W. B. Ozarowski, J. Kuk, E. Davydova and K. Moffat, *Structure*, 2015, **23**, 1179–1189.

32 R. Narikawa, T. Ishizuka, N. Muraki, T. Shiba, G. Kurisu and M. Ikeuchi, *Proc. Natl. Acad. Sci. U.S.A.*, 2013, **110**, 918–923.

33 H. Li, J. R. Zhang, R. D. Vierstra and H. L. Li, *Proc. Natl. Acad. Sci. U.S.A.*, 2010, **107**, 10872–10877.

34 C. C. Cornilescu, G. Cornilescu, E. S. Burgie, J. L. Markley, A. T. Ulijasz and R. D. Vierstra, *J. Biol. Chem.*, 2014, **289**, 3055–3065.

35 D. Bellini and M. Papiz, *Structure*, 2012, **20**, 1436–1446.

36 J. R. Wagner, J. R. Zhang, D. von Stetten, M. Guenther, D. H. Murgida, M. A. Mroginski, J. M. Walker, K. T. Forest, P. Hildebrandt and R. D. Vierstra, *J. Biol. Chem.*, 2008, **283**, 12212–12226.

37 J. Mailliet, G. Psakis, K. Feilke, V. Sineshchekov, L. O. Essen and J. Hughes, *J. Mol. Biol.*, 2011, **413**, 115–127.

38 X. Shu, A. Royant, M. Z. Lin, T. A. Aguilera, V. Lev-Ram, P. A. Steinbach and R. Y. Tsien, *Science*, 2009, **324**, 804–807.

39 S. Bhattacharya, M. E. Auldridge, H. Lehtivuori, J. A. Ihalainen and K. T. Forest, *J. Biol. Chem.*, 2014, **289**, 32144–32152.

40 K. D. Piatkevich, F. V. Subach and V. V. Verkhusha, *Nat. Commun.*, 2013, **4**, 2153.

41 T. Mathes, J. Ravensbergen, M. Kloz, T. Gleichmann, K. D. Gallagher, N. C. Woitowich, R. St. Peter, S. E. Kovaleva, E. A. Stojković and J. T. M. Kennis, *J. Phys. Chem. Lett.*, 2015, **6**, 239–243.

42 A. Björling, O. Berntsson, H. Takala, K. D. Gallagher, H. Patel, E. Gustavsson, R. St. Peter, P. Duong, A. Nugent, F. Zhang, P. Berntsen, R. Appio, I. Rajkovic, H. Lehtivuori, M. R. Panman, M. Hoernke, S. Niebling, R. Harimoorthy, T. Lamparter, E. A. Stojković, J. A. Ihalainen and S. Westenhoff, *J. Phys. Chem. Lett.*, **6**, 3379–3383.

43 C. Song, G. Psakis, C. Lang, J. Mailliet, W. Gärtner, J. Hughes and J. Matysik, *Proc. Natl. Acad. Sci. U.S.A.*, 2011, **108**, 3842–3847.

44 P. Edlund, H. Takala, E. Claesson, L. Henry, R. Dods, H. Lehtivuori, M. Panman, K. Pande, T. White, T. Nakane, O. Berntsson, E. Gustavsson, P. Båth, V. Modi, S. Roy-Chowdhury, J. Zook, P. Berntsen, S. Pandey, I. Poudyal, J. Tenboer, C. Kupitz, A. Barty, P. Fromme, J. Koralek, T. Tanaka, J. Spence, M. Liang, M. Hunter, S. Boutet, E. Nango, K. Moffat, G. Groenhof, J. Ihalainen, E. Stojković, M. Schmidt and

S. Westenhoff, *Sci. Rep.*, 35279.
45 Y. Yang, M. Linke, T. von Haimberger, J. Hahn, R. Matute, L. González, P. Schmieder and K. Heyne, *J. Am. Chem. Soc.*, 2012, **134**, 1408–1411.
46 E. S. Burgie, J. Zhang and R. D. Vierstra, *Structure*, 2016, **24**, 448–457.
47 T. Rohmer, C. Lang, C. Bongards, K. B. S. S. Gupta, J. Neugebauer, J. Hughes, W. Gärtner and J. Matysik, *J. Am. Chem. Soc.*, 2010, **132**, 4431–4437.
48 K. C. Toh, E. A. Stojković, I. H. M. van Stokkum, K. Moffat and J. T. M. Kennis, *Proc. Natl. Acad. Sci. U.S.A.*, 2010, **107**, 9170–9175.
49 K. C. Toh, E. A. Stojković, A. B. Rupenyan, I. H. Van Stokkum, M. Salumbides, M. L. Groot, K. Moffat and J. T. Kennis, *J. Phys. Chem. A*, 2011, **115**, 3778–3786.
50 F. Velazquez Escobar, P. Piwowarski, J. Salewski, N. Michael, M. Fernandez Lopez, A. Rupp, B. Muhammad Qureshi, P. Scheerer, F. Bartl, N. Frankenberg-Dinkel, F. Siebert, M. A. Mroginski and P. Hildebrandt, *Nat. Chem.*, 2015, **7**, 423–430.
51 F. Velazquez Escobar, C. Lang, A. Takiden, C. Schneider, J. Balke, J. Hughes, U. Alexiev, P. Hildebrandt and M. A. Mroginski, *J. Phys. Chem. B*, 2017, **121**, 47–57.
52 P. Schwinté, W. Gärtner, S. Sharda, M.-A. Mroginski, P. Hildebrandt and F. Siebert, *Photochem. Photobiol.*, 2009, **85**, 239–249.
53 P. Piwowarski, E. Ritter, K.-P. Hofmann, P. Hildebrandt, D. von Stetten, P. Scheerer, N. Michael, T. Lamparter and F. Bartl, *ChemPhysChem*, 2010, **11**, 1207–1214.
54 E. A. Stojković, K. C. Toh, M. T. A. Alexandre, M. Baclayon, K. Moffat and J. T. M. Kennis, *J. Phys. Chem. Lett.*, 2014, **5**, 2512–2515.
55 H. Foerstendorf, C. Benda, W. Gärtner, M. Storf, H. Scheer and F. Siebert, *Biochem.*, 2001, **40**, 14952–14959.
56 J. J. van Thor, N. Fisher and P. R. Rich, *J. Phys. Chem. B*, 2005, **109**, 20597–20604.
57 B. Nie, J. Stutzman and A. Xie, *Biophys. J.*, 2005, **88**, 2833–2847.
58 H. Takala, H. Lehtivuori, O. Berntsson, A. Hughes, R. Nanekar, S. Niebling, M. Panman, L. Henry, A. Menzel, S. Westenhoff and J. A. Ihalainen, *J. Biol. Chem.*, 2018, jbc.RA118.001794.
59 H. Lehtivuori, I. Rissanen, H. Takala, J. Bamford, N. V. Tkachenko and J. A. Ihalainen, *J. Phys. Chem. B*, 2013, **117**, 11049–11057.
60 A. K. Covington, M. Paabo, R. A. Robinson and R. G. Bates, *Anal. Chem.*, 1968, **40**, 700–706.
61 Y. Hirose, N. C. Rockwell, K. Nishiyama, R. Narikawa, Y. Ukaji, K. Inomata, J. C. Lagarias and M. Ikeuchi, *Proc. Natl. Acad. Sci. U.S.A.*, 2013, **110**, 4974–4979.
62 H. Takala, H. Lehtivuori, H. Hammar??n, V. P. Hyt??nen and J. A. Ihalainen, *Biochemistry*, 2014, **53**, 7076–7085.
63 D. R. Davydov, E. Deprez, G. H. B. Hoa, T. V. Knyushko, G. P. Kuznetsova, Y. M. Koen and A. I. Archakov, *Arch. Biochem. Biophys.*, 1995, **320**, 330–344.
64 S. Mustalahti, P. Myllyperkiö, T. Lahtinen, K. Salorinne, S. Malola, J. Koivisto, H. Häkkinen and M. Pettersson, *J. Phys. Chem. C*, 2014, **118**, 18233–18239.
65 E. M. S. Maçôas, R. Kananavicius, P. Myllyperkiö, M. Pettersson and H. Kunttu, *J. Phys. Chem. A*, 2007, **111**, 2054–2061.
66 J. Bredenbeck and P. Hamm, *Rev. Sci. Instrum.*, 2003, **74**, 3188–3189.
67 W. Kabsch and IUCr, *J. Appl. Crystallogr.*, 1993, **26**, 795–800.
68 A. J. McCoy, R. W. Grosse-Kunstleve, P. D. Adams, M. D. Winn, L. C. Storoni and R. J. Read, *J. Appl. Crystallogr.*, 2007, **40**, 658–674.
69 G. N. Murshudov, P. Skubák, A. A. Lebedev, N. S. Pannu, R. A. Steiner, R. A. Nicholls, M. D. Winn, F. Long and A. A. Vagin, *Acta Crystallogr. D*, 2011, **67**, 355–367.
70 P. Emsley, B. Lohkamp, W. G. Scott and K. Cowtan, *Acta Crystallogr. D*, 2010, **66**, 486–501.
71 J. J. Snellenburg, S. P. Laptenok, R. Seger, K. M. Mullen and I. H. M. van Stokkum, *J. Stat. Softw.*, 2012, **49**, 1–22.
72 C. Schumann, R. Groß, N. Michael, T. Lamparter and R. Diller, *ChemPhysChem*, 2007, **8**, 1657–1663.
73 M. Linke, Y. Yang, B. Zienicke, M. A. S. Hammam, T. Von Haimberger, A. Zacarias, K. Inomata, T. Lamparter and K. Heyne, *Biophysical Journal*, 2013, **105**, 1756–1766.
74 J. A. Ihalainen, H. Takala and H. Lehtivuori, *Frontiers in Molecular Biosciences*, 2015, **2**, 75.
75 J. Dasgupta, R. R. Frontiera, K. C. Taylor, J. C. Lagarias and R. A. Mathies, *Proc. Natl. Acad. Sci. U.S.A.*, 2009, **106**, 1784–1789.
76 P. W. Kim, N. C. Rockwell, L. H. Freer, C. W. Chang, S. S. Martin, J. C. Lagarias and D. S. Larsen, *J. Phys. Chem. Lett.*, 2013, **4**, 2605–2609.
77 X. Yang, E. A. Stojkovic, J. Kuk and K. Moffat, *Proc. Natl. Acad. Sci. U.S.A.*, 2007, **104**, 12571–12576.